

Advances in Pulsed Doppler Methods for Peripheral Perfusion Imaging

Michael F. Insana
Department of Bioengineering
University of Illinois at Urbana-
Champaign, Urbana, IL, USA
mfi@illinois.edu

Yang Zhu
Department of Bioengineering
University of Illinois at Urbana-
Champaign, Urbana, IL, USA
yangzhu2@illinois.edu

MinWoo Kim
UWAMIT, Dept Bioengineering
University of Washington,
Seattle, WA, USA
mkim180@uw.edu

L. Wawrzyniec Dobrucki
Department of Bioengineering
University of Illinois at Urbana-
Champaign, Urbana, IL, USA
dobrucki@illinois.edu

Abstract—We report on methods for imaging blood perfusion in peripheral skeletal muscle tissues without exogenous contrast enhancement. The ultimate goal is to provide new tools for monitoring the development and treatment of peripheral artery disease (PAD) in diabetic patients. Sparse ultrasonic pulse-echo acquisitions are arranged into 3-D echo data arrays. Each array is decomposed using higher-order singular value decomposition (HOSVD) methods to uncouple echo sources for clutter filtering before signal power is mapped into power Doppler (PD) images. This method enables further segmentation of the blood-echo power into flow maps covering non-overlapping velocity ranges. Our method is compared with other imaging modalities that together assess the recovery in a murine hindlimb ischemia model of PAD.

Keywords—*ischemic tissue assessment, label-free imaging, pulse sampling, SVD clutter filtering, tumor blood flow*

I. INTRODUCTION

Peripheral artery disease (PAD) affects the lives of more than 12 million Americans. The most severe consequence of PAD is critical limb ischemia (CLI) leading to claudication, skin ulcers, and, in some cases, amputations. Patients with CLI also experience higher mortality rates from coronary artery disease and stroke. Treatments range widely from lifestyle changes to peripheral vascular bypass surgery depending on severity. The AHA [1] suggests that effective diagnosis and treatment monitoring of PAD involving CLI should include regular assessments of vascular flow and perfusion at all vascular scales throughout the lower extremities, coupled with evaluations of tissue oxygenation to assess wound healing potential.

US-based ankle-brachial index (ABI) measurements and CT or MR angiography are standard clinical assessments of anatomical obstructions leading to reduced arterial patency in PAD [1]. BOLD-MR and transcutaneous oximetry are applied in some situations to identify hypoxia resulting from ischemic regions. Microvascular flow can be specifically evaluated using molecular imaging probes and contrast media applied to optical [2, 3], nuclear [4], MR [5], and US [6, 7] imaging methods in the lower extremities where the initial effects of PAD are most significant. In addition, new methods involving non-contrast-enhanced Doppler ultrasound for imaging the microvasculature with plane-wave transmits and 2-D SVD clutter filtering [8, 9] are available. SVD is applied to 2-D echo-data arrays arranged into Casorati matrices, where the array axes correspond to spatial and slow time data dimensions.

Our approach records echoes from linear arrays that transmit long sequences (1-10s) of temporally sparse pulse packets (Fig. 1). The received echo signals are arranged into 3-D data arrays that are clutter filtered with a 3-D SVD method that yields sensitive and specific images of tissue perfusion [10, 11]. Tests of these methods using an ischemic animal model at 24 MHz are described below.

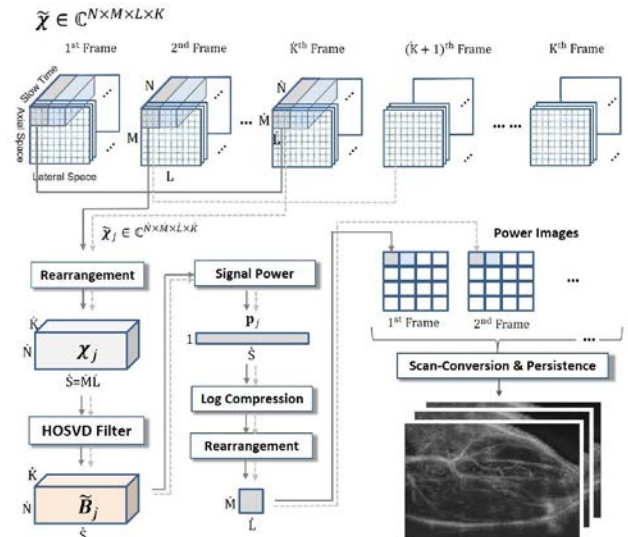


Fig. 1. Summary of the PD perfusion imaging method. 4-D echo acquisitions are rearranged and parsed into 3-D array segments. Each segment is decomposed via HOSVD and filtered to isolate the blood subspace. Signal power is computed and scan converted to form power-Doppler perfusion images (lower right). This figure is from [10].

II. METHODS

A. Surgical Preparation of the Ischemic Hindlimb

A healthy murine model of partial hindlimb ischemia was adopted [12] to study the feasibility of perfusion imaging in vivo during systematic changes in peripheral muscle perfusion. Anesthetized animals placed on a 37°C heating pad have their femoral vasculature exposed through a small incision on the right inner thigh. Dual ligation of the right femoral artery distal to the profundus branch reduced blood flow to the right hindlimb by approximately 50%. The left hindlimb served as a control. Animals were scanned with a laser speckle-contrast imager before and after ligation (Fig. 2) to confirm the

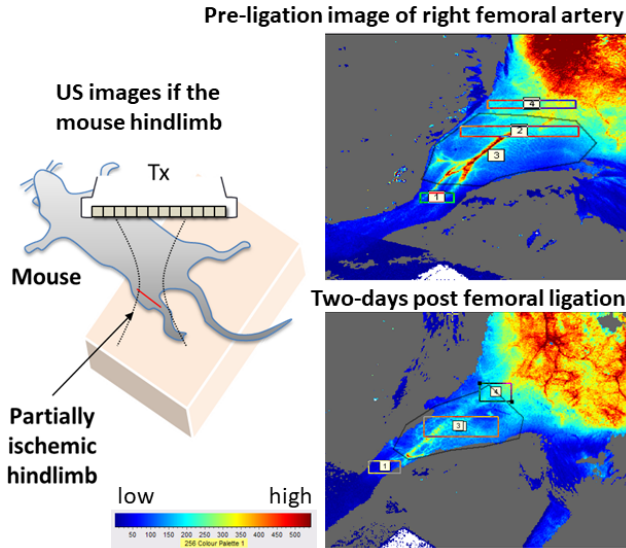


Fig. 2. (left) The scanning geometry for ultrasonic imaging using a linear array transducer. (right) Laser speckle contrast images (LSCI) showing surface flows pre-ligation and two days post-ligation during recovery. The boxes illustrate regions selected for the summary in Fig. 5b. The color bar shows qualitatively how LSCI color indicates flow rates.

occlusion. These measurements were part of a larger multimodality study designed to assess vascular dynamics during induced healthy-state angiogenesis [14].

B. Data Acquisition and PD Image Formation

Focused pulse transmissions yielded echo data recorded from a scan plane along the right and left medial thigh muscle on anesthetized mice lying in a supine position (Fig. 2). Data were recorded immediately prior to surgical ligation, and again at 10 min intervals post-ligation up to 60 min, and at days 1, 3, 7, and 14 post-ligation. Acquisition parameters from a FUJIFILM VisualSonics Vevo 2100 are listed in Table 1.

Table 1. Echo Acquisition Parameters from [10].

Imaging System	Vevo 2100/MS 400 linear array probe
Pulse freq/duration/format	12.5 or 24 MHz/2 cycle/baseband IQ data
Fast-time sampling properties	24Ms/s, $M=200-272$ samples, 6.4-8.7mm
Lateral-sampling properties	16.7 l/mm, $L=240-250$ lines, 14.4-15mm
Slow-time sampling properties	1000 pules/s, $N=17$ pulses rec'ed/frame
Frame-time sampling prop's	9 frames/s, $K\leq 100$ Doppler frames rec'ed

As illustrated in the top row of Fig. 1, we record four dimensions of complex IQ data. The 4-D data arrays correspond to axial and lateral spatial axes with M and L samples, respectively, and slow time and Doppler frame-time axes with

The National Heart, Lung, And Blood Institute of the National Institutes of Health under Award Number R01HL148664 partially supported research reported in this publication. The content is solely the responsibility of the authors and does not necessarily represent the official views of NIH.

All experiments were performed with the approval of the Institutional Animal Care and Use Committee of the University of Illinois at Urbana-Champaign following the principles outlined by the American Physiological Society on research animal use.

N and K samples, respectively. Since we found no characteristic clutter features corresponding to the individual spatial axes, these data were combined into one spatial axis with $S=M\times L$ samples. The S spatial-domain samples were subdivided into overlapping rectangular regions with $\hat{S} \ll S$ samples and separate *spatially adaptive clutter filters* were developed for each subregion. Hence, the echo data being filtered form complex 3-D arrays, $X \in \mathbb{C}^{N \times \hat{S} \times K}$.

The standard assumption is that X is the sum of input from three physical sources: tissue clutter, moving red blood cells, and acquisition noise: $X = C + B + N$. These components overlap in space and time. We strived to uncouple echo sources from each other through HOSVD methods that decompose X into three orthogonal bases, as detailed in [11]:

$$X = \sum_{i_1=1}^N \sum_{i_2=1}^{\hat{S}} \sum_{i_3=1}^K g_{i_1 i_2 i_3} u_{i_1} \times v_{i_2} \times w_{i_3}. \quad (1)$$

Elements g_{i_1, i_2, i_3} collectively form a 3-D *core tensor*, G . These are the singular values resulting from the decomposition. Vectors u, v, w are eigenvectors from the slow-time, spatial, and frame-time data axes, respectively. The sets of eigenvectors are organized into matrices U, V, W . The symbol \times indicates an outer product between two vectors.

Ideally, core tensor G may be represented as the sum of three non-overlapping subspaces, nominally each of size equal to X : $G = G_C + G_B + G_N$. All nonzero elements of G_B are assumed to have zero values in the corresponding elements of G_C, G_N . Hence, core tensor G is similar to echo-array X but now the three contributing sources are more uncoupled. Clutter and noise are filtered from X to give blood-echo-only data array B by including only the nonzero elements of blood-echo subspace G_B in the synthesis of B ,

$$B = \sum_{i_1 i_2 i_3 \in G_B} g_{i_1 i_2 i_3} u_{i_1} \times v_{i_2} \times w_{i_3}. \quad (2)$$

Several practical conditions prevent the echo sources contributing to X from being completely uncoupled. For example, a wideband clutter signal from moving tissue will generate a clutter subspace that overlaps the blood subspace. In addition, iid white-Gaussian noise contributes to each singular value.

Signal power is mapped into PD image pixels as a function of position from the Frobenius norm $\|B\|_F^2$. This process is summarized graphically in Fig. 1 and detailed in [10, 11].

C. Clutter and Noise Filtering

The most challenging aspect of PD imaging is accurate selection of the blood subspace, G_B . We identified five statistical features computed for each singular value within G that identify singular values that are predominantly from the clutter source [11]. As with 2-D SVD, the five features rely on an assumption that clutter is the most echogenic and the lowest-rank component of G , occupying the first few singular values along each of the three core tensor axes. The noise subspace is low amplitude and full rank, so a minimum description length filtering method [13] works well at the blood-noise interfaces in G [11].

D. Validation

Power Doppler (PD) estimates are considered more appropriate than color-flow (CF) estimates for in vivo perfusion assessments because PD estimates are independent of Doppler angle. Unless motion within each spatial region of S samples is predominantly along one direction in the US scan plane, ‘mean velocity’ estimates are not meaningful. PD estimates register motion regardless of Doppler angle but they are intrinsically qualitative, which makes it difficult to validate our methods using PD images. Instead, the methods were validated quantitatively by CF measurements of the velocity of tissue-mimicking (TM) blood flowing slowly through a cluster of fibers oriented along one known direction. The 0.6-mm diameter fibers within a dialysis cartridge shown in Fig. 3 served as a perfusion phantom for quantitative validation.

III. RESULTS

A. Phantom Studies

A calibrated infusion pump controlled the *average flow* of TM blood into the fibers of the dialysis cartridge. The *average speed* of the TM blood through the 20-cm long fibers was measured by measuring the transit time with a stopwatch. After

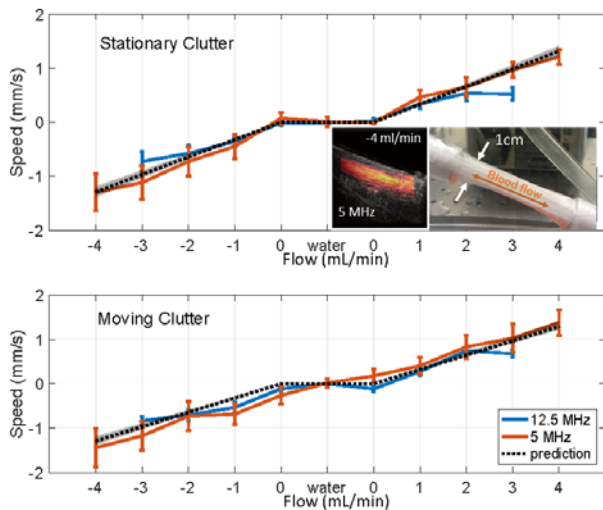


Fig. 3. Measurements of tissue-mimicking blood speed through dialysis cartridge fibers (180 fibers over a 10 mm cross sectional area (see insert) where each fiber has 0.6 mm inner diam.). The dashed line is a measurement made using a calibrated infusion pump and a stopwatch measuring the transit time through the fibers. Measurements with 12.5 MHz and 5 MHz Doppler pulses are made for a Doppler angle of 79° . Negative velocities indicate flow away from the transducer. The ‘water’ measurement is for stationary water in the flow fibers. Those marked ‘0’ include stationary TM blood in the fibers. Error bars indicate ± 1 sd. The data at 12.5 MHz were acquired with the system described in Table 1. The 5 MHz data were acquired with an Ultrasonix Sonix RP system.

clutter and noise filtering, blood echo signals were resynthesized via (2). Computing the spatially-averaged power spectrum over a stationary region of flow, the mean Doppler frequency was found from the spectral centroid. The angle-corrected Doppler equation gave estimates of the mean speed of TM blood flowing in the dialysis cartridge that were compared with stopwatch measurements in Fig. 3. We also compared results to those estimated using a standard lag-one

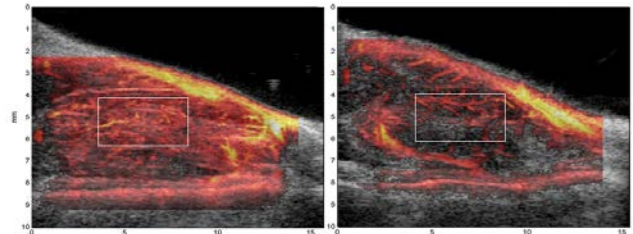


Fig 4. Power Doppler images at 24 MHz of in vivo perfusion in a mouse hindlimb immediately prior to femoral artery ligation (left) and two days post ligation (right). The ROIs above are 10×15 mm. Boxes are examples of ROIs over which the average PD signal plotted in Fig. 5a was measured.

autocorrelator [16] to find statistically equivalent estimates to values shown in Fig. 3.

Velocity measurements at 5 and 12.5 MHz with stationary clutter show that pulsed-Doppler estimates of velocity agree with stopwatch estimates within one standard deviation. At flows greater than 2 ml/min, 12.5 MHz velocity estimates are biased because of aliasing caused by our inability to fully control frame rates. We find similar agreement with moving clutter experiments, although the largest relative errors were found at the slowest flows using 5 MHz pulses. Moving clutter is generated in this phantom when pulses of water from a peristaltic pump were injected at ~ 1 Hz into the dialysis cartridge but outside the cellulose fibers. Velocity estimates show that echo-signal filtering does not greatly distort blood echoes even as it minimizes clutter and noise.

B. PD Imaging of the Ischemic Hindlimb

We evaluated 27 mice over the 14-day ischemia-recovery period. An example of one case showing a pre-ligation image at 24 MHz and another on the same mouse two days post-ligation is found in Fig. 4. Notice how perfusion is originally uniform with few vessels appearing within the perfusion background. Normal vascular flow (Fig. 4, left) is generally too high to register in perfusion images given the parameters we set. Some loss of echo SNR can be seen at depths greater than 7 mm for these 24 MHz pulses, however, the need to visualize microvasculature when possible encourages us to use high frequency pulses in mice.

At two days post-ligation (Fig. 4, right), the average muscle perfusion is at its lowest, at roughly 50% of normal resting perfusion. Flow in the microvasculature is now slow enough to be clearly seen but blood cell movement is patchy. Muscle ischemia varies spatially during the time that arteriogenic and angiogenic processes are rebuilding the vasculature. Although muscle perfusion is lower, surface flows are beginning to return to normal after two days as seen in Fig. 5b.

C. Multimodality Comparisons

To increase confidence that the perfusion patterns seen are representative of tissue changes observed during angiogenic recovery, we compared the ultrasound results to multimodality measurements obtained for the same animals or equivalent cohorts.

Figure 5a compares spatially averaged ultrasonic PD image values measured over a muscle volume (red) with SPECT measurements of tissue hypoxia and angiogenic activity (green). We find with US-PD measurements that during the first hour post ligation, muscle perfusion is reduced only 2 dB ($\sim 20\%$) as tissues reroute flow away from the surface to preserve muscle (Fig. 5b) in response to ischemia. After 2-3 days, compensatory mechanisms in muscle appear to be exhausted: muscle perfusion is about half of the normal values (-6 dB), hypoxia indicators are at maximum values, and angiogenic markers are still increasing (Fig. 5a).

By day 7, tissue hypoxia is reduced as muscle perfusion increases. Angiogenic activity remains high until day 14 when the system has reestablished homeostasis. The photoacoustic measurements in Fig. 5c show a $\sim 20\%$ increase in deoxy-to-oxyhemoglobin ratio between ligation and day 7, consistent

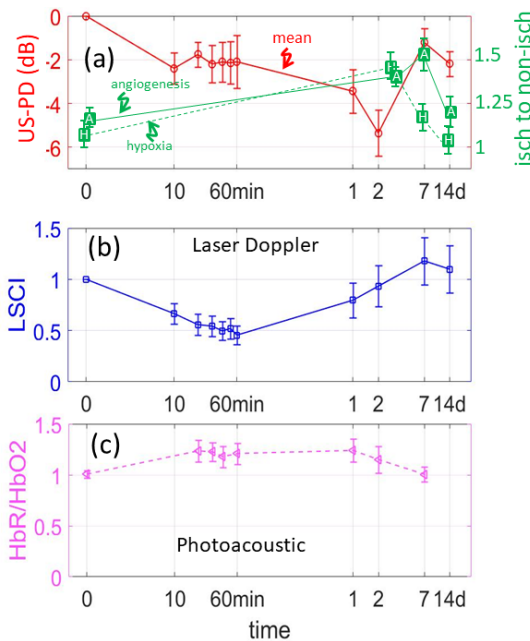


Fig. 5. (a) Measurements of the spatially averaged PD signal (red) at 24 MHz from the region of mouse hindlimb shown in Fig. 4 as a function of log-time post ligation. Values at $t = 0$ are recorded immediately pre-ligation to give the reference (0 dB). Mean values (green) from SPECT images estimate tissue angiogenic response using a ^{99m}Tc -labeled radiotracer targeting $\alpha_v\beta_3$ integrin (NC100692, GE Healthcare, UK) and hypoxic response using ^{99m}Tc -labeled 2-nitroimidazole that is retained in hypoxic tissue (BRU-5921 Bracco USA). Plotted are the ratios of right-to-left hindlimb responses as a function of post-ligation time. A ratio of one indicates equal left-right activity. (b) Laser speckle contrast images (LSCI) show that surface flows also decline to 50% of pre-ligation values but much earlier than that found deeper in ischemic muscle. (c) Photoacoustic image data indicate changes in the ratio of deoxyhemoglobin to oxyhemoglobin in the detected blood signal at the skin surface. Increases in the ratio indicate a hypoxic state that coincides with surface ischemia seen in (b). All data are summarized from [14].

with the SPECT data in Fig. 5a. The results show that a 50% reduction in perfusion results yields only a 20-25% fall in tissue oxygenation.

D. Tumor Imaging

We applied the same PD methods to image a densely vascular melanoma lesion implanted in a mouse in Fig. 6 (from

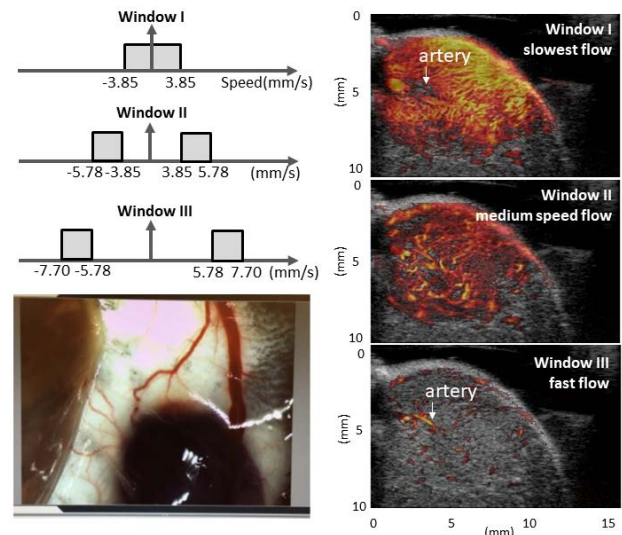


Fig. 6. Images of a mouse melanoma from [11]. US echo data are filtered to remove clutter and noise but, before PD images are formed, the filtered echo data are segmented into velocity ranges shown in the upper left. The PD images show arterial flow at the highest speeds (bottom right) that appear as a “hole” in the PD perfusion image at the lowest speeds (top right). Medium speed flows show larger-size arterioles in this densely vascular tumor. Bottom left is a photo of the exposed melanoma tumor and associated vasculature two weeks after implantation.

[11]). Tumor cells were injected subcutaneously into the flank of male black C57BL/6 mice (Charles River Laboratories, Skokie, IL, USA). Anesthetized mice were scanned with 24 MHz pulses to acquire 3 s of echo data (30 sequential Doppler frames at 10-Hz frame rate). The clutter filter classifier that was trained using simulation data. It was then applied to the tumor data to identify core tensor elements belonging to the clutter subspace. Post filtered echo signals were processed to find the Doppler frequency spectrum. The frequency axis was converted to velocity, and three velocity windows were set to display slow flow $< |3.9|$ mm/s, medium flow $\pm (3.9$ to $5.8)$ mm/s, and fast flow $\pm (5.8$ to $7.7)$ mm/s. The three spectral ranges and the corresponding PD images are shown in Fig. 6.

The power Doppler images show it is possible to segment arterial flow from arteriole flow and capillary perfusion by selecting velocity ranges. Hence, it is possible to select velocity ranges using PD imaging to view flow in various sections of the vascular tree. Because this tumor is so densely vascular, the distinctions can be clearly seen.

IV. DISCUSSION

Our perfusion imaging results are consistent with other imaging modalities that offer different insights into changes in tissue perfusion. Consequently, US-PD imaging may offer an important component to multimodality approaches in the discovery of mechanisms associated with changes in perfusion, specifically, those associated with diabetic-onset PAD.

Our methods extend 2-D SVD clutter filtering methods now widely applied to 2-D Casorati data arrays that are organized along spatial and slow time dimensions. We increase the intrinsic sensitivity and specificity to perfusion echoes by adding Doppler frame-time sampling as the third array

dimension. The echo sources are mostly decoupled for filtering purposes by decomposing data arrays using 3-D SVD. Singular values along the frame-time axis of the core tensor are highly sensitive to slow red blood cell movements, and three basis sets offer new opportunities for separating blood echoes from clutter and noise.

Echo acquisition required to form an image is longer than current methods, ranging from 1-10 s. Long acquisitions offer the advantage of significantly increasing the Doppler frequency resolution, which improves sensitivity of the measurement to slow-moving red blood cells. Consequently, exogenous contrast enhancement is unnecessary. The weakness of the approach is the loss of frame rate. However, since peripheral perfusion in the resting patient is steady over this acquisition time, we can reasonably assume that echo signals are temporally stationary as required for clutter filtering.

While temporally stationary, we found that perfusion is spatially heterogeneous, especially in ischemic tissues (see Fig. 4). Consequently, clutter filters are developed adaptively within regions of interest, which demands significant computational resources. Each frame of PD image now requires at least 19 s on a standard laptop PC. There are many opportunities for increasing the frame rate using GPU and other high-performance computing resources.

The advantages offered by our approach are related to (a) long-duration, sparse pulse sampling and (b) growth of data array dimensions that offer additional eigenbases for clutter filtering. Alternative new techniques are emerging that describe combinations of random sparse sampling and deep learning using fast algorithms that are able to effectively separate microvascular blood flow from clutter and noise [15]. Currently, the method of [15] assumes that the echo data are the sum of a low-rank matrix from clutter and a very sparse matrix from contrast-enhanced ultrasound (CEUS). The high reflectivity of gaseous contrast media provides a sparse random sampling of echoes directly in the spatiotemporal domain. Normal tissue perfusion is not sparse without enhancement, as seen in Figs. 4 and 6, but it could be sparse in some domain, just as a sine wave is dense in time but sparse in the Fourier domain. In that situation, we could change the regular temporal sampling now employed to be randomly sampled in time. Compressive sampling methods would become relevant, thus reducing clutter and noise sampling to a regularized least-squares problem. The general topic of appropriate sampling of compressive signals is a topic of great future interest in many areas of medical sonography.

References

- [1] S. Misra, MH Shishehbor, E.A. Takahashi, et al., "Perfusion assessment in critical limb ischemia: principles for understanding and the development of evidence and evaluation of devices. A scientific statement from the American Heart Association," *Circulation*, vol. 140, (in press), 2019.
- [2] J. Allen, K Howell, "Microvascular imaging: techniques and opportunities for clinical physiological measurements," *Physiol. Meas.* vol. 35, no. 7, pp. R91-R141, 2014.
- [3] O. Mironov, R. Zener, N. Eisenberg, K.T. Tan, G. Roche-Nagle, "Real-time quantitative measurements of foot perfusion in patients with critical limb ischemia," *Vasc. Endovascular Surg.*, vol. 53, no. 4, pp. 310-315, 2019.
- [4] M.R. Stacy, W. Zhou, A.J. Sinusas, "Radiotracer imaging of peripheral vascular disease," *J. Nucl. Med. Technol.* vol. 43, no. 3, pp. 185-192, 2015.
- [5] O.A. Gimnich, J. Singh, J. Bismuth, D.J. Shah, G. Brunner, "Magnetic resonance imaging based modeling of microvascular perfusion in patients with peripheral artery disease," *J Biomech.*, 93:147-158. 2019.
- [6] T. Nguyen, B.P. Davidson, "Contrast enhanced ultrasound perfusion imaging in skeletal muscle," *J. Cardiovasc Imaging*, vol. 27, no. 3, pp. 163-177, 2019.
- [7] C. Huang, P Song, P Gong, J.D. Trzasko, A. Manduca, S. Chen, "Debiasing-based noise suppression for ultrafast ultrasound microvessel imaging," *IEEE Trans. Ultrason. Ferroelectr. Freq. Control*, vol. 66, no. 8, pp. 1281-1291, 2019.
- [8] C. Deme ne, T. Deffieux, M. Pernot, et al., "Spatiotemporal clutter filtering of ultrafast ultrasound data highly increases Doppler and fUltrasound sensitivity," *IEEE Trans. Med. Imaging*, vol. 34, no. 11, pp. 2271-2285, 2015.
- [9] Y.L. Li, D Hyun, L. Abou-Elkacem, J.K. Willmann, J.J. Dahl, "Visualization of small-diameter vessels by reduction of incoherent reverberation with coherent flow power Doppler," *IEEE Trans. Ultrason. Ferroelectr. Freq. Control*, vol. 63, no. 11, pp. 1878-1889, 2016.
- [10] M-W. Kim, C.K. Abbey, J. Hedhli, W.L. Dobrucki, M.F. Insana, "Expanding acquisition and clutter filter dimensions for improved perfusion sensitivity," *IEEE Trans. Ultrason. Ferroelec. Freq. Control*, vol. 64, no. 10, pp. 1429-1438, 2017.
- [11] M-W. Kim, Y. Zhu, J. Hedhli, L.W. Dobrucki, M.F. Insana, "Multi-dimensional clutter filter optimization for ultrasonic perfusion imaging," *IEEE Trans. Ultrason. Ferroelec. Freq. Control*, vol. 65, no. 11, pp. 2020-2029, 2018.
- [12] J. Hua, L.W. Dobrucki, M.M. Sadeghi, et al., "Noninvasive imaging of angiogenesis with a ^{99m}Tc -labeled peptide targeted at $\alpha\text{v}\beta\text{3}$ integrin after murine hindlimb ischemia," *Circulation*, vol. 111, no. 24, pp. 3255-3260, 2005.
- [13] T. Yokota, N. Lee, A. Cichocki, "Robust multilinear tensor rank estimation using higher-order singular value decomposition and information criteria," *IEEE Trans. Signal Process.*, vol. 65, no. 5, pp. 1196-1206, 2017.
- [14] J. Hedhli, M-W Kim, H.J. Knox, J.A. Cole, T. Huynh, M. Schuelke, I.T. Dobrucki, L. Kalinowski, J. Chan, A.J. Sinusas, M.F. Insana, L.W. Dobrucki, "The landmarks of vascular recovery," *Theranostics* (in press).
- [15] O. Solomon, R. Cohen, Y. Zhang, Y. Yang, H. Qiong, J. Luo, J.G. van Sloun, Y.C. Eldar, "Deep unfolded robust PCA with application to clutter suppression in ultrasound," arXiv: 1811.08252v1, 20 Nov 2018.
- [16] C. Kasai, K. Namekawa, A. Koyano, and R. Omoto, "Real-time two-dimensional blood flow imaging using an autocorrelation technique," *IEEE Trans. Sonics Ultrason.*, vol. SU-32, pp. 458-464, 1985.